Article

Exploring the Potential of Portable Spectroscopic Techniques for the Biochemical Characterization of Roots in Shallow Landslides

Lorenzo Marzini [1],*[ID], Daniele Ciofini [2][ID], Juri Agresti [2][ID], Leonardo Ciaccheri [2], Enrico D'Addario [1], Leonardo Disperati [1][ID], Salvatore Siano [2] and Iacopo Osticioli [2],*[ID]

1   Dipartimento di Scienze Fisiche, della Terra e dell'Ambiente, Università degli Studi di Siena, 53100 Siena, Italy
2   Istituto di Fisica Applicata "N. Carrara", Consiglio Nazionale delle Ricerche (IFAC-CNR), 50019 Florence, Italy
*   Correspondence: marzini4@student.unisi.it (L.M.); i.osticioli@ifac.cnr.it (I.O.)

Abstract: In the present work, Raman, Fourier Transform Infrared (FTIR) and elemental Laser-Induced Breakdown Spectroscopy (LIBS) spectroscopic techniques were used for the assessment of the influence of plant root composition towards shallow landslide occurrence. For this purpose, analyses were directly carried out on root samples collected from chestnut forests of the Garfagnana basin (northern Apennines, Italy) in different areas devoid and affected by shallow landslides due to frequent heavy rain events. Results have highlighted a correlation between the biochemical constituents of wooden roots and the sampling areas. In particular, different content of lignin/cellulose, as well as minerals nutrients, have been detected in roots collected where shallow landslides occurred, with respect to more stable areas. The results achieved are in line with the scientific literature which has demonstrated the link between the chemical composition of roots with their mechanical properties and, in particular, tensile strength and cohesion. Finally, portable spectroscopic instrumentations were employed without the need for either any sample preparation for Raman and LIBS spectroscopy or minimal preparation for FTIR spectroscopy. This novel and fast approach has allowed achieving information on the content of the major constituents of the root cell, such as cellulose and lignin, as well as their mineral nutrients. This approach could be reasonably included among the vegetation protection actions towards instability, as well as for the evaluation of shallow landslide susceptibility, combining geological, vegetational and biochemical parameters with sustainability.

Keywords: Raman; FTIR; LIBS; tensile strength; root reinforcement

1. Introduction

Shallow landslides mainly consist of the sliding of poorly cemented material on a shallow planar surface [1]. Usually, these slope failures have a rupture surface that rarely extends beyond a few meters deep, are longer than wider and have a small scar area [2]. Shallow landslides are often triggered by intense rainfall events, and, due to high frequency, high propagation velocity and lack of warning signs represent one of the most dangerous and destructive instability phenomena occurring in the world [3–5].

It is well known that vegetation may play a role towards slope stability [6–11]. Basically, there are two main vegetation effects: hydrological (e.g., reduction of the water pore pressure through tree rainfall interception) and mechanical ones (an increase of the soil strength due to the presence of roots and an increase of the soil shear stress due to vegetation load) [7,12,13]. Regarding soil strength, this property is affected by below-ground tree attributes, as roots provide reinforcement to the soil in terms of additional cohesion (influenced in turn by root strength and root density) [14]. Despite the development over the

years of root bundle models for root reinforcement estimation [15], root density, tensile and pull-out root strength remain key fundamental data for slope stability evaluations [16–18].

Root mechanical properties are provided by structural chemical components organized in complex patterns into the plant cell walls [19]. In detail, it is possible to distinguish two different types of cell walls, named primary and secondary. While primary must be capable of growth (it thus imparts properties of elasticity and flexibility), secondary cell walls are thicker and stiffer and therefore provide strength and stability to the cell and the plant [20]. The structural chemical components responsible for this latter characteristic are primarily lignin, cellulose and hemicellulose and, therefore, these polymers are responsible for the mechanical properties of roots [16,21]. Lignin is a complex polymer formed in the cell walls of vascular plants via free radical coupling reactions between various 4-hydroxycinnamyl alcohols (including coniferyl alcohol-G lignin, sinapyl alcohol-S lignin and *p*-coumaryl alcohol-H lignin) and the growing polymer as an endwise polymerization [22]. The main function of lignin can be expressed as a matrix that holds cellulose fibers together, acting as a bonding and stiffening agent (viscoelastic properties); this role is fundamental within the cell, transferring stress between the hemicellulose matrix and cellulose [22]. Cellulose consists of para-crystalline microfibrils made of β-(1-4)-linked D-glucose that are synthesized at the plasma membrane by CesA complexes. The structure is flat and ribbon-like and is the most abundant polysaccharide in plant cells [23]. Cellulose chains are grouped in a hemicellulose matrix, characterized by a random amorphous structure with small strength. The entire structure is termed microfibril. Each layer of the wood cell wall is made up of many microfibrils arranged in a helical structure; the microfibrils serve as the scaffold that maintains cell wall strength and are cross-linked by matrix polysaccharides [24]. Focusing on cell walls, the microfibril part defines the root morphology [23] and provides resistance to tension and pull-out. Lignin, acting as a matrix, fills the spaces in the cell wall between cellulose, hemicellulose and pectin (a complex branched polysaccharide) and increases the mechanical strength of the cell wall, therefore cascading on the root systems and the soil-root interaction [16].

Most of the shallow landslide susceptibility studies that consider vegetation effects (the beneficial effect provided by the presence of root systems in the soil [8,12,25,26], the adverse effect due to the vegetation load [9,10,27] or the influences of canopy properties towards eco-hydrological slope stability models [28,29]) focus only on the macroscopic effects previously mentioned, disregarding the role of plant roots composition (i.e., lignin, cellulose) and other chemical components (e.g., absorbed minerals).

Moreover, traditional methodologies for the characterization of the biochemical composition of wood components are currently labor-intensive and time-consuming and therefore are not well-suited to handle a large data set. Standard methods developed for biomass characterization often require laborious sample preparation protocols, the use of toxic reagents that may require remediation, long analysis times and complex data processing.

For this reason, the novelty of this work can be assessed from two standpoints: first, the study of the correlation between the biochemical composition of wooden roots and shallow landslides occurring. Second, the original analytical approach being used to determine such a correlation.

In particular, a different analytical approach is herein proposed, which is less invasive, requiring minimal sampling and sample preparation (also avoiding the extraction and chemical treatments), and more representative of the territorial context, allowing more vegetation parameters to be assessed in less time and with reduced experimental costs. In this context, our results suggest that the fast and in situ analysis of root contents in terms of the biochemical composition can further help to discriminate possible shallow landslide-prone areas.

The analytical approach applied in this study is based on the use of spectroscopic techniques, such as Raman, Fourier Transform Infrared spectroscopy (FTIR) and Laser-Induced Breakdown Spectroscopy (LIBS), for the characterization of the chemical composition of plant roots at the molecular and elemental level, respectively. These spectroscopic tech-

niques have been applied to geology [30] and the chemical study of wood and other lignin-containing biomass/biomaterials [31].

Contrary to most studies on slope stability, which are focused on the modelling of root cohesion (an input parameter used in deterministic and probabilistic shallow landslides susceptibility evaluations) [15,32], the spectroscopic approach leads to the identification/quantification of root constituents [16,33], such as cellulose, hemicellulose and lignin, that govern the mechanical traits of roots [34]. In this respect, vibrational spectroscopy (Raman and FTIR) is often used to characterize the chemical compositions of root samples thanks to the high efficiency of both these techniques in quantifying and discriminating among wood organic polymers. Along with the characterization of the molecular composition of roots, the analysis of their mineral nutrition content is also an important parameter for evaluating wood stress. In this regard, high concentrations and/or deficiency of root nutrients can both cause abnormalities in the root cell wall composition (and, consequently, in lignin and cellulose) [35,36]. Some chemical elements are believed to be important influencing agents. As an example, nitrogen and phosphorus regulate cell wall genes involved in pectin modification, cell wall relaxation, hemicellulose/cellulose modification and carbohydrate hydrolytic enzymes. Moreover, literature has reported that calcium (Ca) plays an important role in the biosynthesis of lignin in plants [37], affecting the activity of specific lignin enzymes such as guaiacol-peroxidase (POD), the protein arginine deiminase (PAD) or the phenylalanine ammonia-lyase (PAL) [35].

For this reason, the analytical approach proposed in this work, beyond the analysis at the molecular level (lignin and cellulose) of roots, also considers the evaluation of their mineral nutrition content, leading to a more precise and complete characterization. Analysis of the nutrients of roots is achieved by using the LIBS technique which can provide rapid information regarding the atomic composition of the material without requiring any sample preparation [38,39]. LIBS has been applied for sorting wood waste [40] and, recently, for classifying wood species [41]. Some studies of the application of LIBS on plant roots can be found in the literature focused mainly on the characterization of elemental composition [42–46]. However, to the best of our knowledge, there are no studies in the literature trying to relate the biochemical structure and composition of roots with shallow landslide occurrence. Moreover, this study represents the first attempt to explore the potential of rapid and portable spectroscopic techniques for landslide susceptibility analysis. For this purpose, a field survey was carried out in the Garfagnana basin (northern Apennines, Italy) with the specific aims of (i) collecting root sample data inside, near and far from shallow landslides locations; (ii) analyzing root samples with Raman, FTIR and LIBS techniques; (iii) assessing the possible correlations between structural and compositional root components and shallow landslide occurrence.

2. Results

2.1. FTIR

Representative FTIR spectra of chestnut root samples collected inside, near and far from shallow landslide locations are shown in Figure 1. As far as is known, spectral patterns of wood are characterized by typical broad hydrogen-bonded (O–H) stretching absorption at 3400 cm^{-1}, prominent C–H stretching absorptions around 3000–2800 cm^{-1} and several well-defined peaks in the fingerprint region between 1800 and 600 cm^{-1}. The 1735 cm^{-1} band is characteristic of the non-conjugated carbonyl group (C=O str. of AcO or COOH), and bands at 1600 and 1507 cm^{-1} are ascribable to aromatic skeletal vibrations in lignin. The bands at 1462 (C–H deformation and aromatic skeletal vibrations) and 1425 cm^{-1} (C–H in-plane deformation) also make a significant contribution from lignin [47,48]. Further important bands are at 1375 (C–H in-plane deformation for polysaccharides), 1330 (syringyl ring breathing and C–O stretching, CH$_2$ def. of cellulose), 1250 cm^{-1} guaiacyl ring breathing and C–O stretching, 1158 cm^{-1} C–O–C antisymmetric bridge stretching vibration in cellulose and hemicellulose, 1120 cm^{-1} C–O–C symmetric stretching and aromatic C–H

in-plane deformation and glucose ring vibration, 1020–1040 cm^{-1} C–O and O–H association bands in cellulose and hemicelluloses and 898 cm^{-1} C–H deformation of cellulose [49,50].
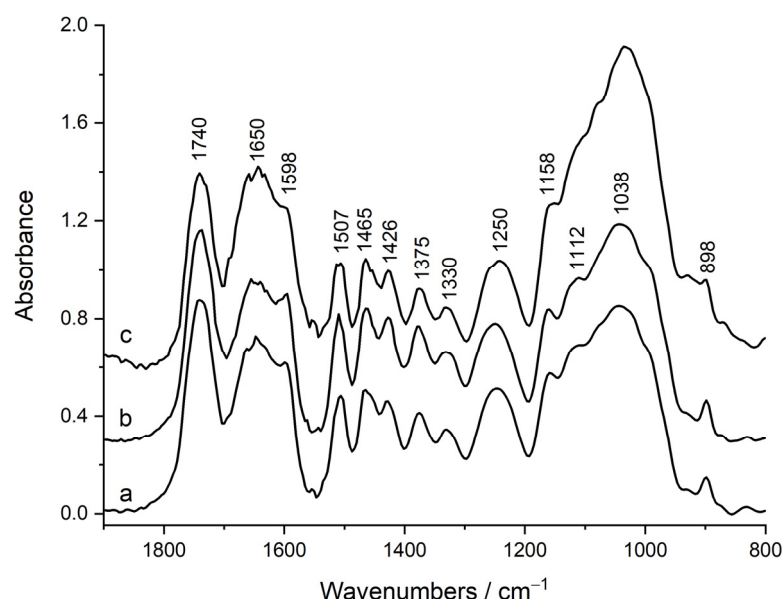

Figure 1. Examples of infrared FTIR spectra (SNV and baseline corrected) of chestnut samples representing the three location types, which are "INSIDE" (**a**), "NEAR" (**b**) and "FAR" (**c**) from the shallow landslide location.

To get semi-quantitative information on the lignocellulosic content of the root samples, the intensity ratios of the absorption maxima at 1507 cm^{-1} (specific absorbance of C=C stretching for aromatic skeletal in lignin) and those associated with carbohydrates were calculated (cellulose and hemicellulose). In this way, any spectral contribution from non-structural components of the woody material (i.e., extractives, mineral substances) was thoroughly minimized. FTIR results, in terms of lignin/carbohydrate ratios, are reported in Figure 2. As shown, the lignin/cellulose content steadily increased toward the region of the slope failure. Basically, the relative change in the L/C ratio is mostly due to an increase of the lignin band at 1507 cm^{-1} and an overall slight decrease of cellulose-hemicellulose bands in the region of the slope failure. The ANOVA test was performed on FTIR data, confirming the statistical validity and veracity of the results achieved. *p* values obtained from ANOVA are as follows (L = 1507, lignin band): L/1465 = 0.112; L/1425 = 0.024; L/1370 = 0.063; L/1247 = 0.016; L/1168 = 0.032; L/1121 = 0.071; L/1030 = 0.122.

2.2. Raman

Selected Raman spectra acquired on chestnut root samples collected inside, near and far from shallow landslides are shown in Figure 3. A total of 90 Raman spectra were acquired, SNV was normalized, adaptive baseline was subtracted and smoothed.

Analogously to what was done with FTIR spectra to get semi-quantitative information on the lignocellulosic content, the intensity ratio of lignin/cellulose was also investigated in Raman spectra. Unfortunately, the Raman band at 1505 (lignin) is very weak and the band at 1160 cm^{-1} (cellulose) is a shoulder compromising the quantification procedure. For this reason, semi-quantitative information was achieved using the Raman bands at 1098 and 1125 cm^{-1} for cellulose and at 1663 cm^{-1} for lignin. These bands are ascribable to the C–C and C–O stretching vibration due to skeletal deformation in cellulose and to the ring-conjugated C=C stretching vibration of sinapyl alcohol and C=O stretching vibration of sinapaldehyde in lignin [24].
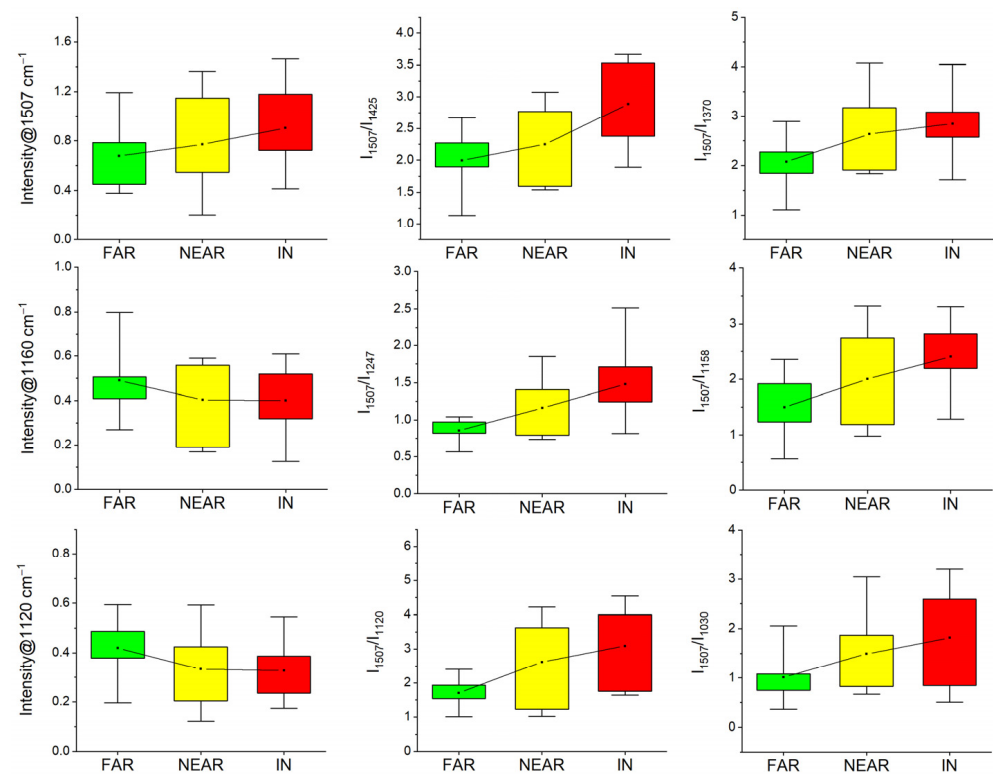
Figure 2. Boxplots of FTIR data showing band intensity variations of lignin and cellulose, along with their ratios, in the three main data acquisition location types ("FAR"—green boxplot, "NEAR"—yellow boxplot and "IN"—red boxplot locations). The box represents data within the first and the third quartile, dot symbol represents the mean value, lines extending parallel from the box are the whiskers in the 10–90 range.
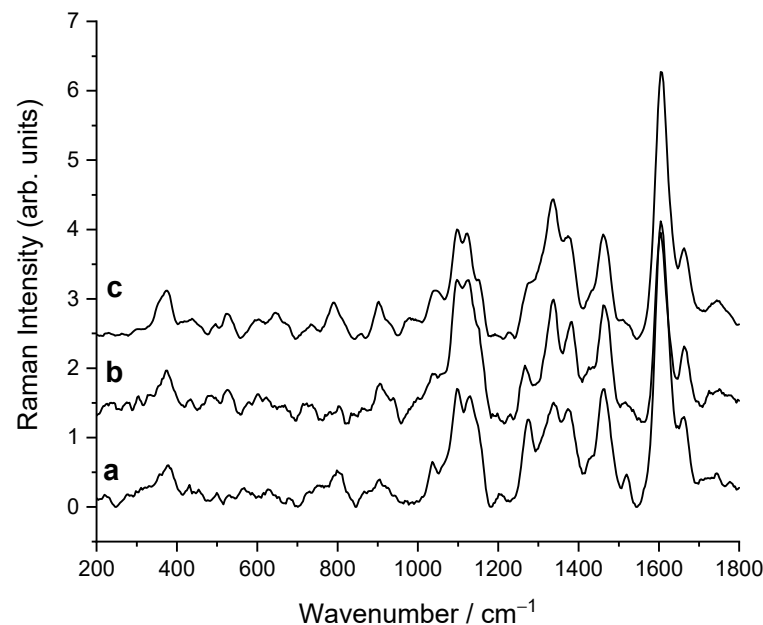

Figure 3. Raman spectra (SNV and baseline corrected) of chestnut samples collected inside (**a**), near (**b**) and far (**c**) from the shallow landslide location.

Similarly to what was observed for FTIR, plots of Figure 4 show a slight decrease of cellulose from "FAR" to "IN" datasets, considering both the band at 1098 and 1125 cm^{-1} (Figure 4a,c, respectively). In contrast, lignin values appear to be stable among the three

groups (Figure 4e). As regards the lignin/cellulose ratio, higher values were observed in the "IN" dataset, considering both the Raman bands ascribable to cellulose (Figure 4b,d). Mean values related to the Raman bands of lignin cellulose and the lignin/cellulose ratios are shown in Table 1 for the three groups. Moreover, the results of ANOVA tests performed on the Raman data were reported in the table to further demonstrate the veracity of the results achieved.
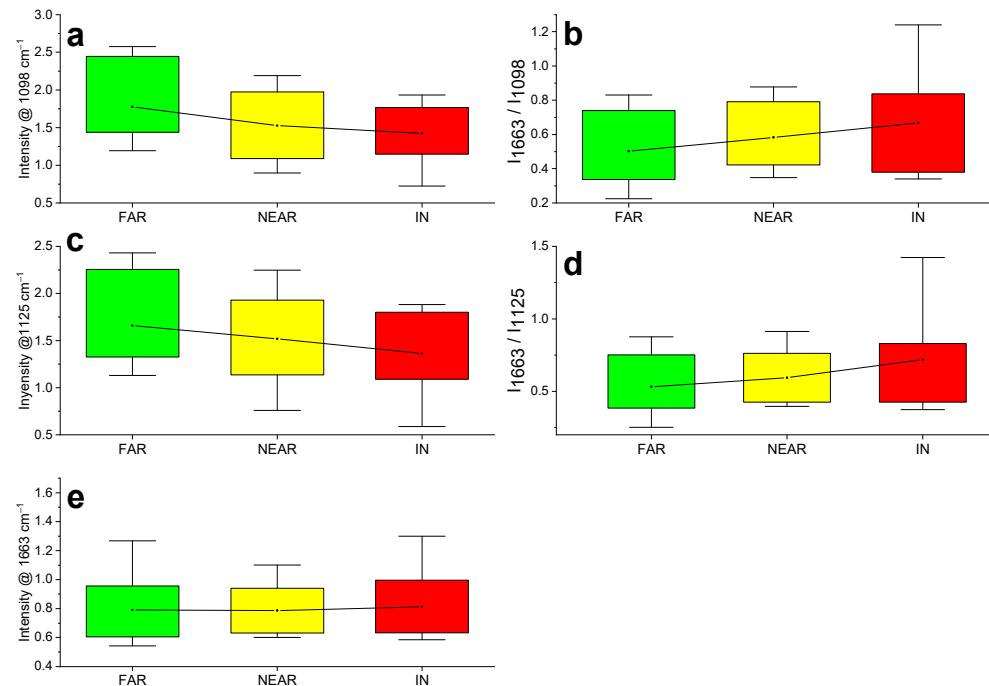

Figure 4. Raman data in terms of 1098 (cellulose, (**a**)), 1125 (cellulose, (**c**)), 1663 cm^{-1} (lignin, (**e**)) and lignin/cellulose ratios (1663/1098) (**b**), (1663/1125) (**d**) considering the three main data acquisition location types ("FAR"—green boxplot, "NEAR"—orange boxplot and "IN"—red boxplot locations). The box represents data within the first and the third quartile, the dot symbol represents the mean value and lines extending parallel from the box are the whiskers in the 10–90 range.

Table 1. Mean values for the whisker plots shown in Figure 4.

Raman Frequencies	Assignment	Datasets Mean Values			ANOVA Test (*p* Value)
		FAR	**NEAR**	**IN**	
1663	lignin	0.79	0.79	0.81	/
1098	cellulose	1.78	1.53	1.42	0.037
1125	cellulose	1.66	1.52	1.36	0.070
1663/1098	lignin/cellulose	0.50	0.58	0.67	0.106
1663/1125	lignin/cellulose	0.53	0.59	0.72	0.098

In our previous work, the dependence of the laser heating temperature on the chemical composition of the material analyzed during Raman measurements was demonstrated [51]. In particular, it was observed that the presence of metal impurities can drastically affect the temperature heating of the material under laser irradiation. For this reason, laser heating temperatures were measured for all three sets of root samples ("IN", "FAR" and "NEAR"). Figure 5 shows the profiles of temperature reached by the sample due to laser irradiation during Raman measurements. A temperature curve was achieved for each sample belonging to the "IN" (red), "NEAR" (yellow) and "FAR" (green) groups, which means a total of 30 temperature profiles. No differences among the samples were observed. Most of the parts of the roots showed temperature values between 38 and 50 °C

independently of the collecting area. To deepen this aspect of the research, a more sensitive spectroscopic technique than T-controlled Raman spectroscopy was used.
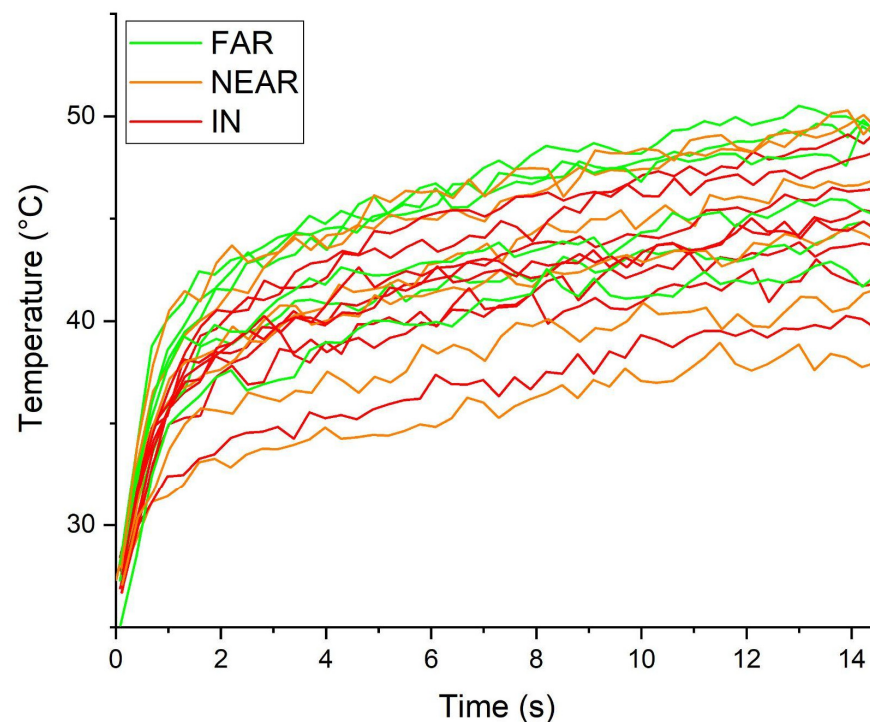

Figure 5. Temperature profiles of the root samples collected inside, near and far from the shallow landslide location.

2.3. LIBS

Spectroscopic data underwent background subtraction, normalization and averaging, resulting in five representative spectra for each sample (see Section 4.2 for details). Three typical root LIBS spectra obtained, averaging five representative spectra for each group, are shown in Figure 6. LIBS atomic bands of the principal constituents and nutrients for plants were selected in the spectra. In particular, emission lines of C I (247.9 nm), Si I (288.2 nm), Fe I (275 nm), Al I (309.3 nm), Ca II (393.36 nm), Mg I (285.29 nm), Na I (589.20 nm), Mn II (294.92 nm), N II (4 closely-spaced lines around 500 nm) and CN molecular violet bands (386–389 nm) were considered for the analysis. These lines were selected on the basis of their good signal-to-noise ratio and for their not-overlapped position with other bands. Spectral information for selected features was obtained using the NIST Atomic Spectra Database. Taking into account that measurements were performed in air, the signals of C and N are likely to be affected by the environmental condition. In order to estimate the contribution of the ambient gas on the C and N (and CN) intensities, 100 LIBS measurements were taken on a pure copper sample, keeping the same acquisition parameters as for the root samples. The integral of the same lines of C, Cn and N were then compared with the signal from the root samples. The air signals of C and CN are far below the corresponding signals in roots, whereas the N signal is of comparable intensity and is therefore shown in Figure 6 for comparison.

Figure 7 shows the whiskers plots of the area of the peaks of the chemical elements selected in Figure 6.
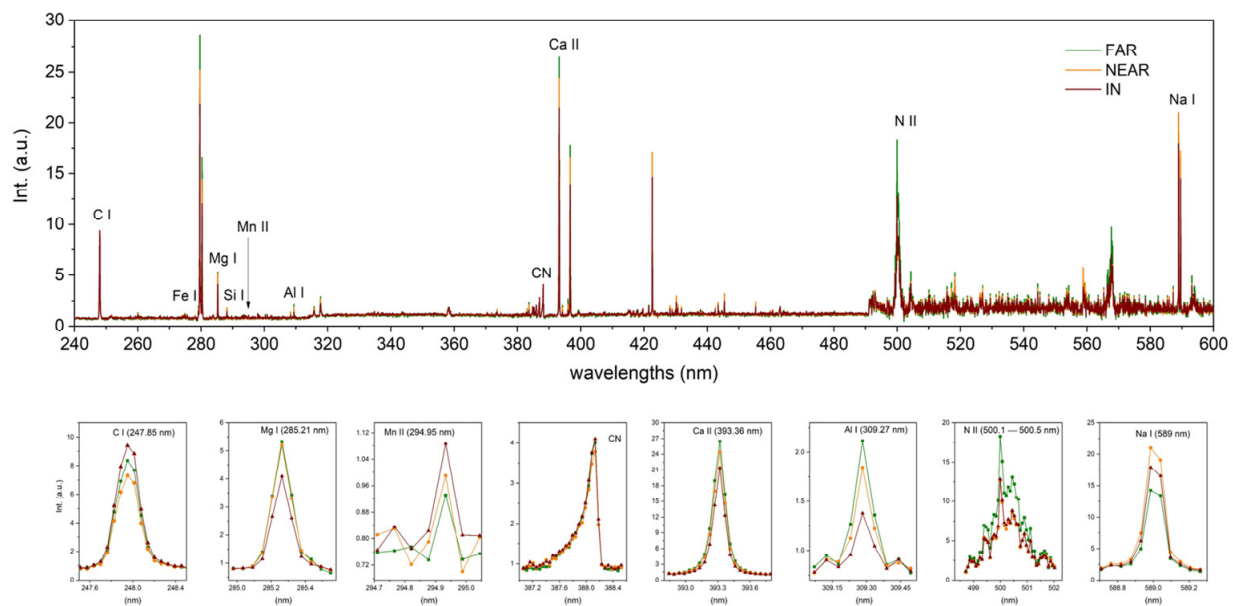
Figure 6. Example of averaged LIBS spectra of chestnut samples collected inside, near and far from the shallow landslide location with identified spectral features. Panels below show some of the selected peaks in larger scale.

Signals of Mg, Ca, Mn, Na, N and Al are statistically different between the "IN" population and "FAR" population (according to two-sample *t*-test at 0.05 significance level), whereas the other signals (C, CN, Fe, Si), despite showing trends among different locations, do not provide statistically significant discrimination capabilities taken singularly. Therefore, we performed LDA analysis which transforms the input features into a lower dimensional space to maximize the ratio of the between-class variance to the within-class variance, thereby guaranteeing maximum class separability. We restricted the analysis to the extreme classes "IN" and "FAR". Performing a 5-fold cross-validation analysis to prevent overfitting, an overall discriminant accuracy of 97% was achieved with a positive predictive value (PPV) of 100% and 97% for the classes "FAR" and "IN", respectively. PLS-DA over the whole spectrum was also tested for discriminating LIBS signals of the different regions. PLS-DA is a classical method in multivariate analysis that maximizes the covariance between the latent variables and the responses. The PLS-DA model requires an optimal number of components for the considered data set. In this case, 10-fold cross-validation has been used to select the optimal number of PLS components. The best result has been achieved with 7 PLS components achieving an average accuracy of 97%. Table 2 summarizes the results of PLS-DA analysis reporting standard figures of merit in classification analysis (Sensitivity = TP/(TP + FN), Specificity = TN/(TN + FP), Efficiency = $\sqrt{}$(Sensitivity × Specificity)), where samples belonging to a certain class are designated as true positive (TP) if they are correctly recognized by the model, and false negative (FN) if they are erroneously rejected. Correspondingly, samples not belonging to the class of interest are labelled as false positive (FP) if they are erroneously assigned to the class, and true negative (TN) if they are correctly refused.
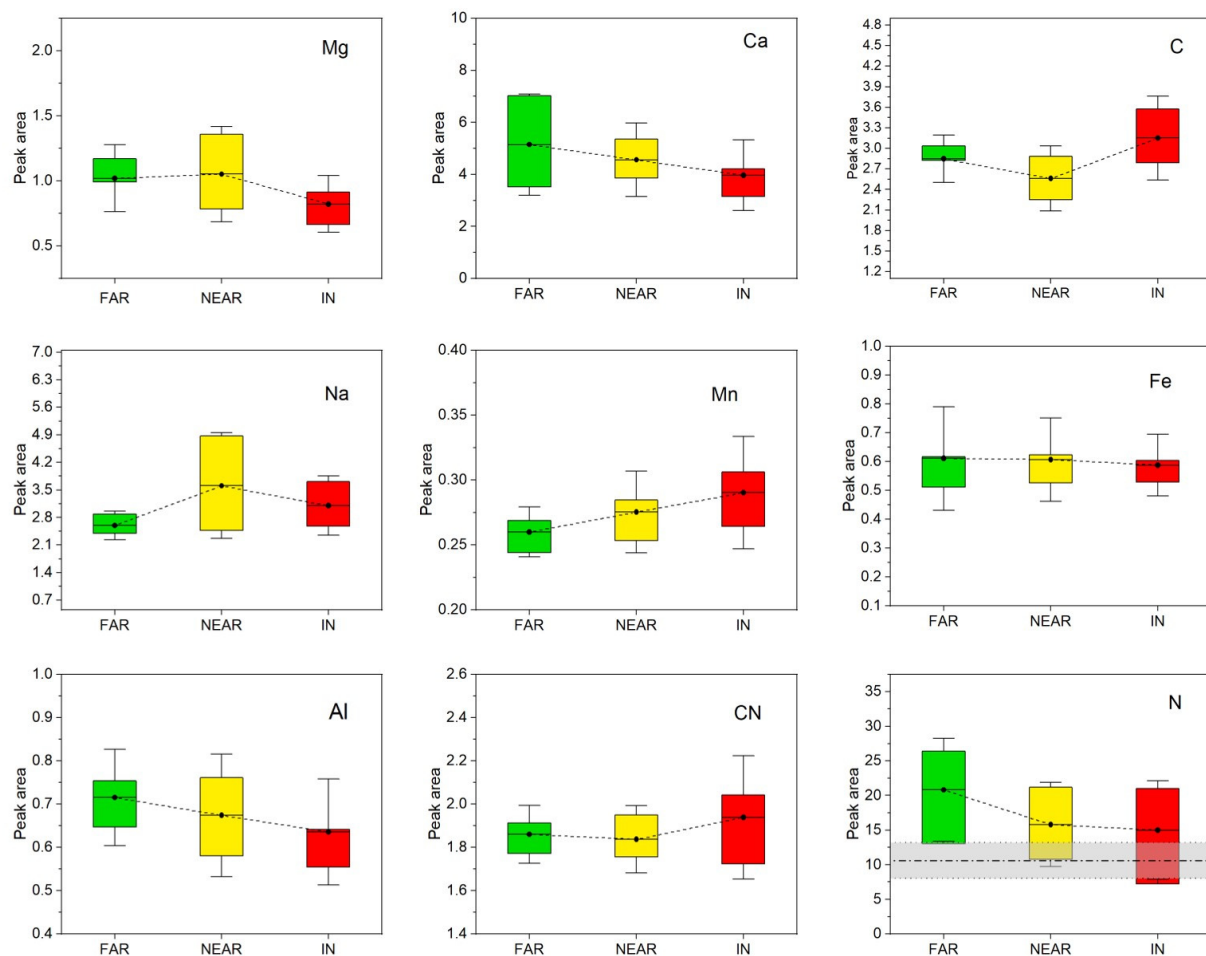
Figure 7. Whisker plots of the area of the LIBS atomic lines of some mineral nutrients detected in the root sections, considering the three main data acquisition location types ("FAR"—green color, "NEAR"—yellow color and "IN"—red color locations). Box represents data within the first and the third quartile, the dot symbol represents the mean value and lines extending parallel from the box represent the standard deviation. Horizontal gray band in the nitrogen (N) plot marks the mean and standard deviation of the signal measured on a pure copper sample.

Table 2. PLS-DA classification figures of merit.

Figures of Merit	FAR	IN	Total
Sensitivity (%)	93	98	97
Specificity (%)	98	93	97
Efficiency (%)	96	96	97

3. Discussion

FTIR and Raman box and whisker plots (Figures 2 and 4) have shown a progressive increase in the L/C ratio moving from stable areas ("FAR") to the shallow landslide locations ("IN"). This change is due to lower cellulose contents in the region of slope failure, as well as to a major lignin content observed by FTIR. Similar to FTIR, Raman plots highlighted a decrease in the cellulose content in the presence of shallow landslides. However, the Raman lignin bands at 1606 and 1663 cm^{-1} remain stable in the three groups. This difference could be explained because vibrational bands in a range of 1600–1700 cm^{-1} are ascribable to lignin, as well as to wood extractives (as tannins, phlobaphenes, alkaloids, phenols, polyphenols), which are probably the most responsible for the stability, whereas

the FTIR band at 1507 can be mainly ascribed to lignin. To confirm this hypothesis, FTIR bands at 1606 and 1663 cm^{-1} were exploited, leading to trends as stable as the Raman ones.

Trying to provide a solid and clear explanation of the decreasing cellulose content in shallow landslides is a very difficult task and the literature itself is misleading in that regard. As an attempt, the main results found in the literature are herein reported. The cellulose content in roots can be affected by a water deficit; cellulose biosynthesis is correlated to soil water content and environmental conditions, as shown in several different species, including Arabidopsis, tobacco suspension cells, grape leaves and wheat roots [52]. For instance, an increased level of UDP-Glc in the expression of *SuSy* (sucrose synthase) and UDP-glucose pyrophosphorylase (*UGPase*) encoding genes was observed in cotton under drought stress, suggesting a potentially higher cellulose biosynthesis [52].

According to the literature, L/C ratio is associated with root tensile strength. Differences in both lignin and cellulose contents can simultaneously affect the L/C ratio and change the root tensile strength and, consequently, root cohesion [53]. Root tensile strength can increase with a higher percentage of both cellulose and lignin [34,54]. Genet et al. studied the correlation between root strength and diameter, showing that roots with smaller diameter had greater tensile strength (and increased cellulose content) [16]; however, in this study, the equivalent lignin content was not assessed. In contrast, the spectroscopic approaches used in our study allowed for obtaining both lignin and cellulose quantification. Lignin content is indeed of primary importance to determine the wood strength and its rate of decomposition; the higher the lignin content the greater the strength of the roots, as well as the slower their degradation [34].

Zhang et al. [33] measured the lignin, cellulose and alpha-cellulose content of different species; by correlating the results with the corresponding tensile strength, authors showed that lignin content increased with the increase in tensile strength. Moreover, the cellulose contents decreased with the increasing of tensile strength (in contrast to results reported by Genet et al. [16]). Lignin may be the main load-bearing element of the wall matrix; our results showed that L/C ratio decreased moving from the shallow landslides ("IN") to stable areas ("FAR"), as further evidence of the possible fundamental role of lignin in the biomechanical roots traits. From the perspective of the spatial variability of root contents, some similarities with our approach can be found in the work of Hales et al. [55] where the influence of topographic positions on the distribution and strength of roots in a debris-flow-prone landscape was studied [55]. According to these results, the topographic position significantly affected cellulose contents (and tensile strength coupled with root cohesion), as nose locations had significantly higher cellulose content than hollows. These results agree with the work of Dietrich et al., which states that landslides most commonly occur in topographic convergent zones (i.e., hollows) [56].

Results achieved in our work are also in line with studies that consider more traditional variables such as, for example, root density (frequently named in literature RAR, Root Area Ratio [6]), root strength and root cohesion [8,11,15], which are all parameters commonly considered (along with soil thickness, soil cohesion, angle of internal friction, etc. [32]) in the physical methods used to assess landslide susceptibility. In the work by Roering et al., the position, along with the characteristics of trees, represented a first-rate parameter in the study of the spatial variability of root strength, as well as of shallow landslides occurring in forests [11]. In other words, root strength could be predicted by mapping the presence of trees on potentially unstable slopes and landslide events observed mainly in areas with reduced root strength (which is in line with a lower cellulose content in the "IN" locations in our work), suggesting that vegetation distribution plays an important role. Moreover, Moos et al. found that susceptibility to landslides was higher in zones with low root reinforcement (which correspond to "IN" locations in our study) [57].

LIBS results show relatively high Ca content in stable areas and a decrease in unstable "IN" locations (i.e., shallow landslides) (Figure 7), confirming the importance of this nutrient related to lignin and cellulose production and root elongation [58–60]. Manganese (Mn) element is linked to the functioning of PAL (the enzyme responsible for the initiation of the

phenylpropanoid pathway and the subsequent increase in the concentration of biophenols-lignin) [61]. The LIBS signal of Mn increases from "FAR" to "IN" areas in accordance with the increase in lignin content, as measured by FTIR. Magnesium (Mg) is a nutrient involved in the vegetation gene connected with the adaptation to the fluctuating environment [62]. As an example, it has been observed that Mg deficiency elicits an alteration of circadian clock gene expression in the roots of Arabidopsis thaliana, a crucial gene expression also present in human cells, mouse fibroblasts, marine unicellular alga and a filamentous fungus. In this context, higher contents observed in "NEAR" and "FAR" locations can be evaluated in terms of better root adaptive capacity. Moreover, according to literature, the concentration of soluble Al in acid soils (favorable soils for chestnut tree development) is linked to stimulation of root growth [63], and LIBS data were able to distinguish the "IN" population from "FAR" populations. A higher signal of C (and accordingly CN) in "IN" location types could be correlated with the mentioned higher content of lignin in those locations. Focusing on nitrogen, LIBS results highlight higher contents moving from "IN" to "FAR" locations. This element has been proven to act as a regulating factor conditioning root system architecture and cascading, lateral root development [64]. In this context, the high signal of this nutrient in stable areas (FAR) can be explained in terms of better lateral root development; the latter is of crucial importance in root reinforcement evaluations [10].

4. Materials and Methods

4.1. Root Sampling

Root sampling was performed in the Garfagnana basin in northern Apennines (Italy; Figure 8). The area extends for about 240 km^2 along the Serchio River valley, parallel to the eastern margin of the Alpi Apuane and the northern Apennines Ridge, reaching the maximum altitude of about 2000 m a. s. l. The tectonic setting of the Garfagnana basin can be described as a graben located within a series of NW–SE-oriented extensional structures that dissect the contractional structures related to the Apennine orogeny [65–68].

The geology of the basin includes almost all the tectonic units (Ligurian and Sub-ligurian Units, the Tuscan Nappe and the Tuscan Metamorphic Units) that make up the northern Apennines (Figure 9) [69]. These units are overlined by Pliocene to Holocene lacustrine and fluvial deposits. The most widely exposed formation in the study area (about 45%) is the silico clastic Macigno arenaceous flysch, consisting of thick layers of sandstone with siltstone and subordinate pelitic interbeds [70]. Climatic conditions are directly related to the morphological features present in the study area; indeed, Alpi Apuane exerts a shielding action towards Atlantic and Mediterranean humid air flows, with a consequent condensation, which results in heavy rainy events [3]. The rainfall regime of the study area can be ascribed to the Apennine-Mediterranean type, with dry summers and cold winters [3]. In detail, the mean annual rainfall is greater than 1600 mm [71] with maximum precipitation from October to March, and the mean annual temperature is 9 °C. About 81% of the study area is covered by forests, which are mainly represented by broadleaf forests with chestnut (*Castanea sativa* Mill.), beech (*Fagus sylvatica* L.) and oaks (*Quercus* spp.) being the dominant species, and needle leaf forests dominated by Norway spruce (*Picea abies* (L.) H. Karst.). Due to this environmental context, chestnut roots were selected as the study species. Roots of chestnuts (about 20–30 years old) were sampled according to different location types (Figure 9) to investigate the role of root components towards shallow landslide occurrences (Table 3).

Roots were extracted from the soil through the excavating of vertical trenches [72]; roots pieces about 50 cm long were cut using sharp scissors to avoid the effect of pre-stress. Roots were then put into sealed plastic bags and transported to the laboratory in a refrigerated box at a temperature of 4 °C to maintain the roots' freshness [6]. Zhang et al. [33] reported that root moisture content has a large impact on the variability of root tensile strength. This emphasizes the need to avoid desiccation during testing. Before spectroscopic measurements, root sections of 0.7–0.8 cm of chestnut were made in the laboratory.
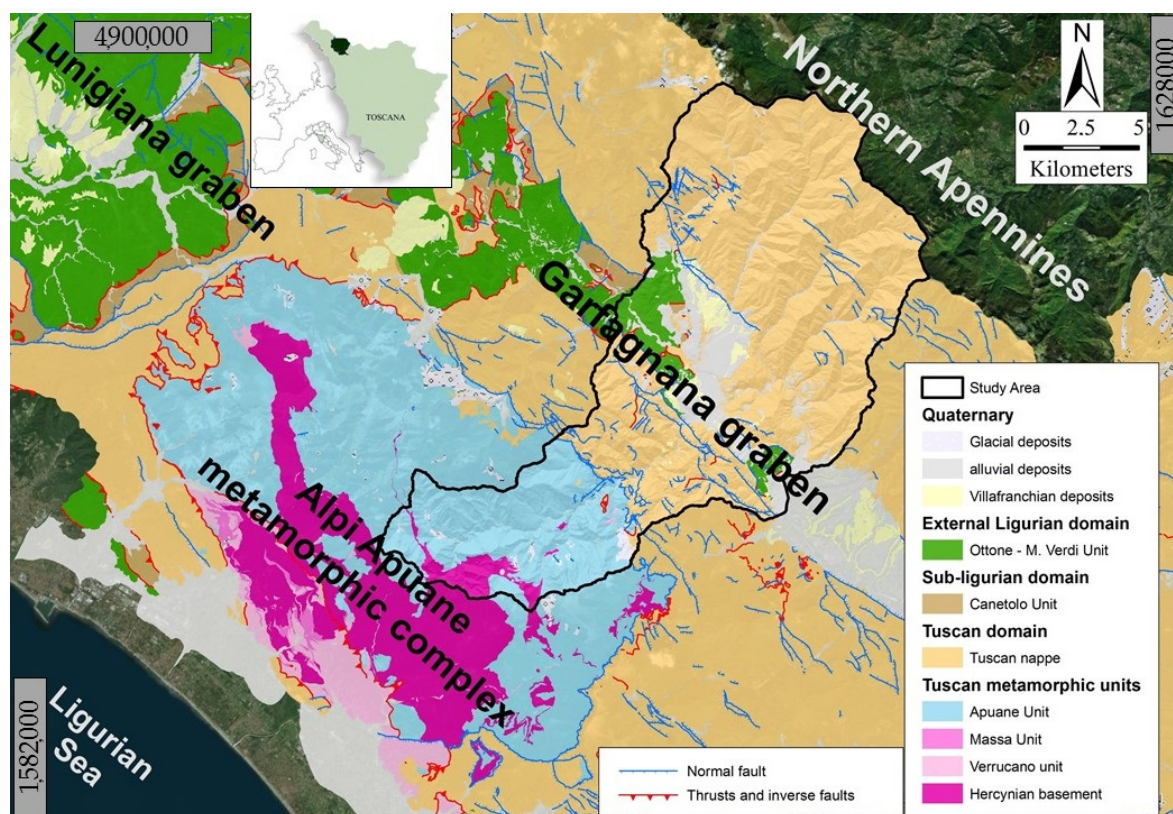
Figure 8. Location and tectonic setting of the study area (coordinate system: Gauss-Boaga, west zone).
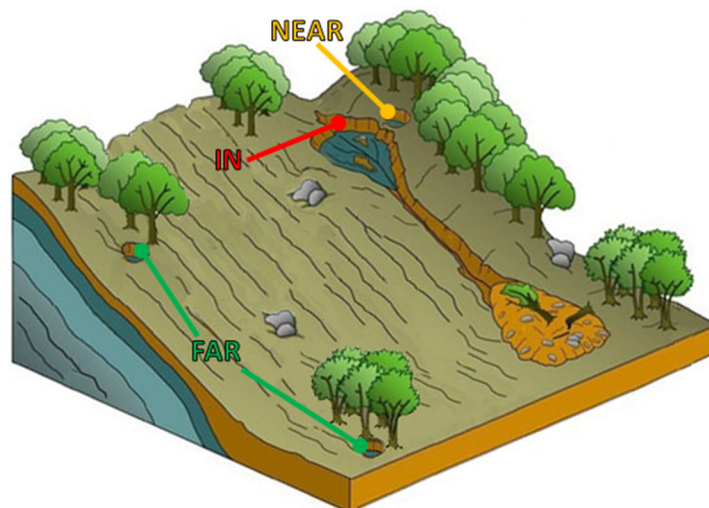

Figure 9. Root sample acquisition field strategy adopted during the survey. Root samples acquired inside ("IN"), near ("NEAR") and far ("FAR"; <1 km) from shallow landslide locations (the latter detected using a landslide inventory) [70].

Table 3. Number of samples according to the sampling scheme adopted in this work.

Location Types	Description	Number of Samples
IN	inside the shallow landslide	10
NEAR	in the neighbour of a shallow landslide (within 10 m)	10
FAR	far from shallow landslides (i.e., stable locations)	10

4.2. Spectroscopic Analysis

Raman analysis was directly carried out on root sections using a homemade portable spectrometer, coupled with a CW laser emitting at 1064 nm [73]. The active spectral range is 185–1850 cm^{-1} with a spectral resolution of 8 cm^{-1}. The focused laser beam at the surface sample has a dimension of 500 μm. For the analysis, an acquisition time of 15 s and an average of 20 acquisitions were used. To improve statistics, three Raman acquisitions were carried out for each root sample in three different areas.

LIBS measurements were performed by using homemade instrumentation, reported previously [74,75]. It consists of a small fiber-coupled endpiece, which includes beam delivery optics, and an instrumental module enclosing the laser excitation source (SSD QS Nd:YAG @1064 nm (Quantel USA, Bozeman, MT, USA) and a set of four compact spectrometers (Avantes B.V., Apeldoorn, The Netherlands) equipped with CCD detector arrays. The system covers the spectral range 200–630 nm with a resolution better than 0.2 nm. The laser spot on the sample has a diameter of about 300μm and the energy per pulse amounts to 20 mJ. LIBS spectra acquisition was activated by a homemade optical trigger board driven by the laser emission, and the integration time was set to 2 ms. Random LIBS scans over root areas using 50 laser shots were carried out on the root section surfaces to overcome the punctual nature of the technique.

FTIR analysis was carried out using an Agilent Cary 630 FTIR portable spectrometer (Agilent Technologies, Santa Clara, CA, USA [76]). KBr disks containing small root pieces (KBr pellet method, [77,78]) were prepared for the analysis. In detail, disk preparation was carried out using an agate mortar with a root/KBr disk ratio of about 2:100. Disks were then put into a steel cylinder and placed under a press (8 atm) for about 1 min. Finally, the resulting compact and transparent tablets were placed into the spectrometer and analyzed.

The decision to work in transmission mode with FTIR was taken after not-successful experiments in reflectance mode configuration due to high absorption and very low signals. Sample preparation adoption was very minimal. The traditional procedure adopted to prepare KBr disks using bulky and heavy presses was not employed in this case. Conversely, very small disks (⌀= 3 mm) were prepared. A small bag (20 × 20 × 7 cm) less than 1 kg contained everything needed for the sample preparation (metal disks, press and mortar). In this condition, 5 min were usually needed for the sample preparation which could potentially be done very easily and in situ.

4.3. Data Processing and Statistical Analysis

Raman and FTIR Spectra were presented following a preprocessing based on Standard Normal Variate (SNV) correction and baseline subtraction. After baseline subtraction, the intensity of spectroscopic bands of lignin and cellulose were studied separately and correlated to assess biochemical changes as a function of root sampling location.

LIBS spectra were processed using the following steps. Each spectrum was background-subtracted using a filter based on a Statistics-sensitive Nonlinear Iterative Peak-clipping algorithm (SNIP) [79] and then normalized to the total intensity. The resulting spectra were finally averaged by groups of ten, thus achieving five representative spectra for each sample. The integrated intensities of the emission lines of C (247.9 nm), Si (288.2 nm), Fe (275 nm), Al (309.3 nm), Ca (422.41 nm), Mg (285.29 nm), Na (589.20), Mn (295.01) and CN molecular violet bands (386–389 nm) were calculated for each averaged spectrum and used as features in the assessment of root characteristics in different locations of shallow landslides. In particular, we tested two standard supervised machine learning (ML) classification techniques to investigate the capability of LIBS data to discriminate root from inside ("IN") from the root from far ("FAR") from the landslide. We performed linear discriminant analysis (LDA) on the dataset of the nine extracted features and partial least squares discriminant analysis (PLS-DA) using the entire spectrum as input.

Statistical and classification analyses were performed using Origin 2018 (Origin Lab Corporation, Northampton, MA, USA, 2018) and Matlab 2022.

5. Conclusions

This work provides new insight into the correlation between root reinforcement and shallow landslides. In particular, the biochemical composition of roots taken from different locations (inside, nearby and far from shallow landslides) was characterized using portable molecular and atomic spectroscopic techniques. This is a novel analytical approach compared to the most traditional ones based on physical models. Differences in terms of lignin, cellulose and nutrient contents moving from unstable (i.e., shallow landslides) to more stable locations were observed using Raman, FTIR and LIBS spectroscopies. In particular, Raman and FTIR analysis highlighted an increase of cellulose content moving from unstable to stable areas. Moreover, an increase in the lignin content was detected by FTIR in unstable areas. The analysis of root nutrients by LIBS showed trends in Mg, Ca, Mn, Al and C signals, possibly related to root vitality and mechanical properties moving from shallow landslides to stable locations. LIBS technique combined with two classification algorithms (LDA and PLS-DA) showed great potential in discriminating between more stable locations and locations more prone to instability by direct analysis of root samples. Both classification models allowed a satisfactory classification of root samples, reaching an accuracy of 97%. On the basis of experimental results obtained in this work, spectroscopic portable techniques might be suitable to detect differences in the biochemical composition of wood depending on vegetational parameters, as well as provide information for shallow landslide prediction. Further insights will be dedicated to the refinement of the laboratory methodology and the definition of an in situ procedure to extend the potential application of this approach for different study areas affected by shallow landslides and for different vegetation types.

Author Contributions: Conceptualization, L.D., I.O. and L.M.; methodology, L.M., I.O., J.A. and D.C.; software, I.O., J.A., L.C. and D.C.; validation, L.M., I.O., J.A. and D.C.; formal analysis, L.M., I.O., J.A. and D.C.; investigation, L.M., I.O., J.A., L.C. and D.C.; resources, L.D.; data curation, L.M., I.O., J.A., E.D., L.C. and D.C.; writing—original draft preparation, L.M.; writing—review and editing, L.M., I.O., J.A., D.C., E.D., L.D. and S.S.; visualization, equal contribution of all authors; supervision, S.S. and L.D.; project administration, L.D.; funding acquisition, S.S. and L.D. All authors have read and agreed to the published version of the manuscript.

Data Availability Statement: All data generated or analyzed for this study are included in this article, and the related datasets are available from the corresponding author upon reasonable request.

Conflicts of Interest: The authors declare no conflict of interest.

References

1. Hungr, O.; Leroueil, S.; Picarelli, L. The Varnes classification of landslide types, an update. *Landslides* **2014**, *11*, 167–194. [CrossRef]
2. Milledge, D.G.; Bellugi, G.; McKean, J.A.; Densmore, A.L.; Dietrich, W.E. A multidimensional stability model for predicting shallow landslide size and shape across landscapes. *J. Geop. Res. Earth Surf.* **2014**, *119*, 2481–2504. [CrossRef]
3. Giannecchini, R.; Galanti, Y.; D'Amato Avanzi, G. Critical rainfall thresholds for triggering shallow landslides in the Serchio River Valley (Tuscany, Italy). *Nat. Hazards Earth Syst. Sci.* **2012**, *12*, 829–842. [CrossRef]
4. Meisina, C.; Scarabelli, S. A comparative analysis of terrain stability models for predicting shallow landslides in colluvial soils. *Geomorphology* **2007**, *87*, 207–223. [CrossRef]
5. Persichillo, M.G.; Bordoni, M.; Meisina, C.; Bartelletti, C.; Barsanti, M.; Giannecchini, R.; D'Amato Avanzi, G.; Galanti, Y.; Cevasco, A.; Brandolini, P.; et al. Shallow landslides susceptibility assessment in different environments. *Geomat. Nat. Hazards Risk* **2017**, *8*, 748–771. [CrossRef]

6. Bischetti, G.B.; Chiaradia, E.A.; Simonato, T.; Spaziali, B.; Vitali, B.; Vullo, P.; Zocco, A. Root strength and root area ratio of forest species in Lombardy (Northern Italy). *Plant Soil* **2005**, *278*, 11–22. [CrossRef]

7. Dazio, E.P.R.; Conedera, M.; Schwarz, M. Impact of different chestnut coppice managements on root reinforcement and shallow landslide susceptibility. *For. Ecol. Manag.* **2018**, *417*, 63–76. [CrossRef]

8. Giadrossich, F.; Schwarz, M.; Cohen, D.; Cislaghi, A.; Vergani, C.; Hubble, T.; Phillips, C.; Stokes, A. Methods to measure the mechanical behavior of tree roots: A review. *Ecol. Eng.* **2017**, *109*, 256–271. [CrossRef]

9. Greenwood, J.R.; Norris, J.E.; Wint, J. Assessing the contribution of vegetation to slope stability. *Proc. Inst. Civ. Eng.—Geotech. Eng.* **2004**, *157*, 199–207. [CrossRef]

10. Kokutse, N.K.; Temgoua, A.G.T.; Kavazović, Z. Slope stability and vegetation: Conceptual and numerical investigation of mechanical effects. *Ecol. Eng.* **2016**, *86*, 146–153. [CrossRef]

11. Roering, J.J.; Schmidt, K.M.; Stock, J.D.; Dietrich, W.E.; Montgomery, D.R. Shallow landsliding, root reinforcement, and the spatial distribution of trees in the Oregon Coast Range. *Can. Geotech. J.* **2003**, *40*, 237–253. [CrossRef]

12. Bischetti, G.B.; Chiaradia, E.A.; Epis, T.; Morlotti, E. Root cohesion of forest species in the Italian Alps. *Plant Soil* **2009**, *324*, 71–89. [CrossRef]

13. Li, Y.; Wang, Y.; Ma, C.; Zhang, H.; Wang, Y.; Song, S.; Zhu, J. Influence of the spatial layout of plant roots on slope stability. *Ecol. Eng.* **2016**, *91*, 477–486. [CrossRef]

14. Vergani, C.; Giadrossich, F.; Buckley, P.; Conedera, M.; Pividori, M.; Salbitano, F.; Rauch, H.S.; Lovreglio, R.; Schwarz, M. Root reinforcement dynamics of European coppice woodlands and their effect on shallow landslides: A review. *Earth-Sci. Rev.* **2017**, *167*, 88–102. [CrossRef]

15. Schwarz, M.; Preti, F.; Giadrossich, F.; Lehmann, P.; Or, D. Quantifying the role of vegetation in slope stability: A case study in Tuscany (Italy). *Ecol. Eng.* **2010**, *36*, 285–291. [CrossRef]

16. Genet, M.; Stokes, A.; Salin, F.; Mickovski, S.B.; Fourcaud, T.; Dumail, J.-F.; van Beek, R. The influence of cellulose content on tensile strength in tree roots. *Plant Soil* **2005**, *278*, 1–9. [CrossRef]

17. Danjon, F.; Barker, D.H.; Drexhage, M.; Stokes, A. Using three-dimensional Plant Root Architecture in Models of Shallow-slope Stability. *Ann. Bot.* **2008**, *101*, 1281–1293. [CrossRef]

18. Moresi, F.V.; Maesano, M.; Matteucci, G.; Romagnoli, M.; Sidle, R.C.; Mugnozza, G.S. Root Biomechanical Traits in a Montane Mediterranean Forest Watershed: Variations with Species Diversity and Soil Depth. *Forests* **2019**, *10*, 341. [CrossRef]

19. Gierlinger, N.; Schwanninger, M. The potential of Raman microscopy and Raman imaging in plant research. *J. Spectrosc.* **2007**, *21*, 498206. [CrossRef]

20. Somssich, M.; Khan, G.A.; Persson, S. Cell wall heterogeneity in root development of *Arabidopsis*. *Front. Plant Sci.* **2016**, *7*, 1242. [CrossRef]

21. Rivera, J.R.; Terrazas, T. Lignin Analysis by HPLC and FTIR. In *Xylem: Methods and Protocols, Methods*; de Lucas, M., Etchells, J.P., Eds.; Springer Science+Business Media LCC.: Berlin/Heidelberg, Germany, 2017; Volume 1544, pp. 193–211.

22. Stark, N.M.; Yelle, D.J.; Agarwal, U.P. Techniques for characterizing lignin. In *Lignin in Polymer Composites*; Faruk, O., Mohini, S., Eds.; Elsevier: Amsterdam, The Netherlands, 2016; pp. 49–66.

23. O'Neill, M.A.; York, W.S. The composition and structure of plant primary cell wall. In *The Plant Cell Wall*; Rose, J.K.C., Ed.; Balckwell Publishing: Oxford, UK, 2003.

24. Zhang, X.; Chen, S.; Xu, F. Combining Raman Imaging and Multivariate Analysis to Visualize Lignin, Cellulose, and Hemicellulose in the Plant Cell Wall. *J. Vis. Exp.* **2017**, *124*, 1–7. [CrossRef]

25. Reubens, B.; Poesen, J.; Danjon, F.; Geudens, G.; Muis, B. The role of fine and coarse roots in shallow slope stability and soil erosion control with a focus on root system architecture: A review. *Trees* **2007**, *21*, 385–402. [CrossRef]

26. Masi, E.B.; Segoni, S.; Tofani, V. Root Reinforcement in Slope Stability Models: A Review. *Geosciences* **2021**, *11*, 212. [CrossRef]

27. Coppin, N.J.; Richards, I.G. *Use of Vegetation in Civil Engineering*; Butterworth-Heinemann: Oxford, UK, 1990.

28. Gonzalez-Oullari, A.; Mickovski, S.B. Hydrological effect of vegetation against rainfall-induced landslides. *J. Hydrol.* **2017**, *549*, 374–387. [CrossRef]

29. Zimmermann, A.; Zimmermann, B. Requirements for throughfall monitoring: The roles of temporal scale and canopy complexity. *Agric. For. Meteorol.* **2014**, *189–190*, 125–139. [CrossRef]

30. Indelicato, C.; Osticioli, I.; Agresti, J.; Ciofini, D.; Mencaglia, A.; Perotti, M.; Viti, C.; Moreschi, R.; Siano, S. Exploring grain sizing of sedimentary calcareous rocks using Raman spectroscopy. *Eur. Phys. J. Plus* **2022**, *137*, 359. [CrossRef]

31. Agarwal, U.P. FT–Raman Investigation of Milled-Wood Lignins: Softwood, Hardwood, and Chemically Modified Black Spruce Lignins. *J. Wood Chem. Technol.* **2011**, *31*, 324–344. [CrossRef]

32. Murgia, I.; Giadrossich, F.; Mao, Z.; Cohen, D.; Capra, G.F.; Schwarz, M. Modeling shallow landslides and root reinforcement: A review. *Ecol. Eng.* **2022**, *181*, 106671. [CrossRef]

33. Zhang, C.; Li-Hua, C.; Jing, J. Why fine tree roots are stronger than thicker roots: The role of cellulose and lignin in relation to slope stability. *Geomorphology* **2014**, *206*, 196–202. [CrossRef]

34. Zhu, J.; Wang, Y.; Mao, Z.; Langendoen, E.J. How does root biodegradation after plant felling change root reinforcement to soil? *Plant Soil* **2020**, *446*, 211–227. [CrossRef]

35. Moura, J.C.; Bonine, C.A.; de Oliveira Fernandes Viana, J.; Dornelas, M.C.; Mazzafera, P. Abiotic and biotic stresses and changes in the lignin content and composition in plants. *J. Integr. Plant Biol* **2010**, *52*, 360–376. [CrossRef] [PubMed]

36. Ogden, M.; Hoefgen, R.; Roessner, U.; Persson, S.; Khan, G.A. Feeding the Walls: How Does Nutrient Availability Regulate Cell Wall Composition? *Int. J. Mol. Sci.* **2018**, *19*, 2691. [CrossRef] [PubMed]

37. Lautner, S.; Ehlting, B.; Windeisen, E.; Rennenberg, H.; Matyssek, R.; Fromm, J. Calcium nutrition has a significant influence on wood formation in poplar. *New Phytol.* **2007**, *173*, 743–752. [CrossRef] [PubMed]

38. Nicolodelli, G.; Cabral, J.; Menegatti, C.R.; Marangoni, B.; Senesi, G.S. Recent advances and future trends in LIBS applications to agricultural materials and their food derivatives: An overview of developments in the last decade (2010–2019). Part I. Soils and fertilizers. *TrAC Trends Anal. Chem.* **2019**, *115*, 70–82. [CrossRef]

39. Senesi, G.S.; Cabral, J.; Menegatti, C.R.; Marangoni, B.; Nicolodelli, G. Recent advances and future trends in LIBS applications to agricultural materials and their food derivatives: An overview of developments in the last decade (2010–2019). Part II. Crop plants and their food derivatives. *TrAC Trends Anal. Chem.* **2019**, *118*, 453–469. [CrossRef]

40. Solo-Gabriele, H.M.; Townsend, T.G.; Hahnc, D.W.; Moskal, T.M.; Hosein, N.; Jambeck, J.; Jacobi, G. Evaluation of XRF and LIBS technologies for on-line sorting of CCA-treated wood waste. *Waste Manag.* **2004**, *24*, 413–424. [CrossRef]

41. Cui, X.; Wang, Q.; Zhao, Y.; Qiao, X.; Teng, G. Laser-induced breakdown spectroscopy (LIBS) for classification of wood species integrated with artificial neural network (ANN). *Appl. Phys. B* **2019**, *125*, 56. [CrossRef]

42. Arantes De Carvalho, G.G.; Bueno Guerra, M.B.; Adame, A.; Nomura, C.S.; Oliveira, P.V.; Pereira De Carvalho, H.W.; Santos, D.; Nunes, L.C.; Krug, F.J. Recent Advances in LIBS and XRF for the Analysis of Plants. *J. Anal. At. Spectrom.* **2018**, *33*, 919–944. [CrossRef]

43. Wang, J.; Shi, M.; Zheng, P.; Xue, S.; Peng, R. Quantitative Analysis of Ca, Mg, and K in the Roots of Angelica Pubescens f. Biserrata by Laser-Induced Breakdown Spectroscopy Combined with Artificial Neural Networks. *J. Appl. Spectrosc.* **2018**, *85*, 190–196. [CrossRef]

44. Liu, F.; Shen, T.; Kong, W.; Peng, J.; Zhang, C.; Song, K.; Wang, W.; Zhang, C.; He, Y. Quantitative Analysis of Cadmium in Tobacco Roots Using Laser-Induced Breakdown Spectroscopy with Variable Index and Chemometrics. *Front. Plant Sci.* **2018**, *9*, 1–12. [CrossRef]

45. Shukla, N.; Bharti, A.S.; Srivastava, S.; Uttam, K.N. Determination of Elements in Carrot Root by Laser Induced Breakdown Spectroscopy. *Natl. Acad. Sci. Lett.* **2017**, *40*, 47–51. [CrossRef]

46. Wang, W.; Kong, W.; Shen, T.; Man, Z.; Zhu, W.; He, Y.; Liu, F. Quantitative Analysis of Cadmium in Rice Roots Based on LIBS and Chemometrics Methods. *Environ. Sci. Eur.* **2021**, *33*, 1–14. [CrossRef]

47. Pandey, K.K. A Study of chemical structure of soft and hardwood and wood polymers by FTIR spectroscopy. *J. Appl. Polym. Sci.* **1999**, *71*, 1969.e75. [CrossRef]

48. Pandey, K.K. Study of the effect of photo-irradiation on the surface chemistry of wood. *Polym. Degrad. Stab.* **2005**, *90*, 9–20. [CrossRef]

49. Moore, A.K.; Owen, N.L. Infrared Spectroscopic Studies of Solid Wood. *Appl. Spectrosc. Rev.* **2001**, *36*, 65–86. [CrossRef]

50. Chang, T.C.; Chang, H.T.; Wu, C.L.; Chang, S.T. Influences of Extractives on the Degradation of Wood. *Polym. Degrad. Stab.* **2010**, *95*, 516–521. [CrossRef]

51. Ciofini, D.; Agresti, J.; Mencaglia, A.A.; Siano, S.; Osticioli, I. Temperature sensing during Raman Spectroscopic of lead white films in different purity grades and boundary conditions. *Sens. Actuators B* **2020**, *325*, 128958. [CrossRef]

52. Le Gall, H.; Philippe, F.; Domon, J.-M.; Gillet, F.; Pelloux, J.; Catherine Rayon. Cell Wall Metabolism in Response to Abiotic Stress. *Plants* **2015**, *4*, 112–166. [CrossRef]

53. Commandeur, P.R.; Pyles, M.R. Modulus of elasticity and tensile strength of Douglas fir roots. *Can. J. For. Res.* **1991**, *21*, 48–52. [CrossRef]

54. Hairiah, K.; Widianto, W.; Suprayogo, D.; Van Noordwijk, M. Tree Roots Anchoring and Binding Soil: Reducing Landslide Risk in Indonesian Agroforestry. *Land* **2020**, *9*, 256. [CrossRef]

55. Hales, T.C.; Ford, C.R.; Hwang, T.; Vose, J.M.; Band, L.E. Topographic and ecologic controls on root reinforcement. *J. Geophys. Res. Earth Surf.* **2009**, *114*. [CrossRef]

56. Dietrich, W.E.; Wilson, C.J.; Reneau, S.L. Hollows, colluvium, and landslides in soil-mantled landscapes. *Hillslope Process.* **1986**, *27*, 362–368. [CrossRef]

57. Moos, C.; Bebi, P.; Graf, F.; Mattli, J.; Rickli, C.; Schwarz, M. How does forest structure affect root reinforcement and susceptibility to shallow landslides? *Earth Surf. Process. Landf.* **2016**, *41*, 951–960. [CrossRef]

58. Elle, O.; Richter, R.; Vohland, M.; Weigelt, A. Fine root lignin content is well predictable with near-infrared spectroscopy. *Sci. Rep.* **2019**, *9*, 6396. [CrossRef]

59. Lupoi, J.S.; Healey, A.; Singh, S.; Sykes, R.; Davis, M.; Lee, D.J.; Shepherd, M.; Simmons, B.A.; Henry, R.J. High-Throughput Prediction of *Acacia* and Eucalypt Lignin Syringyl/Guaiacyl Content Using FT-Raman Spectroscopy and Partial Least Squares Modeling. *BioEnergy Res.* **2015**, *8*, 953–963. [CrossRef]

60. Johanson, L.; Joham, H.E. The influence of sodium on the calcium nutrition of excised cotton roots. *Plant Soil* **1971**, *35*, 323–336. Available online: https://www.jstor.org/stable/42932952 (accessed on 15 April 2023). [CrossRef]

61. Vidović, N.; Pasković, I.; Lukić, I.; Žurga, P.; Majetić Germek, V.; Grozić, K.; Cukrov, M.; Marcelić, Š.; Ban, D.; Talhaoui, N.; et al. Biophenolic Profile Modulations in Olive Tissues as Affected by Manganese Nutrition. *Plants* **2021**, *10*, 1724. [CrossRef]

62. Panter, P.E.; Muranaka, T.; Cuitun-Coronado, D.; Graham, C.A.; Yochikawa, A.; Kudoh, H.; Dodd, A.N. Circadian regulation of the plant transcriptome under natural conditions. *Front. Genet.* **2019**, *10*, 1239. [CrossRef]

63. Bojórquez-Quintal, E.; Escalante-Magaña, C.; Echevarría-Machado, I.; Martínez-Estévez, M. Aluminum, a friend or foe of higher plants in acid soils. *Front. Plant Sci.* **2017**, *8*, 1767. [CrossRef]

64. Sun, C.-H.; Yu, J.-H.; Hu, D.-J. Nitrate: A crucial signal during lateral roots development. *Front. Plant Sci.* **2017**, *8*, 485. [CrossRef]

65. Boschetti, T.; Toscani, L.; Barbieri, M.; Mucchino, C.; Marino, T. Low entalphy Na-chlorine waters from the Lunigiana and Garfagnana grabens: Northern Apenninnes, Italy: Tracing fluid connections and basement interaction via chemical and isotopic composition. *J. Volcanol. Geotherm. Res.* **2017**, *348*, 12–25. [CrossRef]

66. Di Naccio, D.; Boncio, P.; Brozzetti, F.; Pazzaglia, F.J.; Lavecchia, G. Morphotectonic analysis of the Lunigiana and Garfagnana grabens (northern Apennines, Italy): Implication for active normal faulting. *Geomorphology* **2013**, *201*, 293–311. [CrossRef]

67. Eva, E.; Solarino, S.; Boncio, P. HypoDD relocated seismicity in northern Apennines (Italy) preceding the 2013 seismic unrest: Seismotectonic implications for the Lunigiana-Garfagnana area. *Boll. Di Geofis. Teor. Ed Appl.* **2014**, *55*, 739–754. [CrossRef]

68. Carmignani, L.; Decandia, F.A.; Disperati, L.; Fantozzi, P.L.; Kliegfield, R.; Lazzarotto, A.; Liotta, D.; Meccheri, M. Inner Northern Apennines. In *Anatomy of an Orogen: The Apennines and the Adjacent Mediterranean Basins*; Springer: Berlin/Heidelberg, Germany, 2001; pp. 197–214. [CrossRef]

69. Puccinelli, A.; D'Amato Avanzi, G.; Perilli, N. Note Illustrative della Carta Geologica d'Italia alla Scala 1:50,000: Foglio 250 Castelnuovo di Garfagnana. 2014; ISPRA, Progetto CARG. Available online: https://www.isprambiente.gov.it/Media/carg/toscana.html (accessed on 15 April 2023).

70. D'Addario, E. A New Approach to Assess the Susceptibility to Shallow Landslides at Regional Scale as Influenced by Bedrock Geo-Mechanical Properties. Ph.D. Thesis, University of Siena, Siena, Italy, 2021.

71. Nardi, R. Il rischio idrogeologico in Italia: Cause e conseguenze. Il ruolo e le attività dell'Autorità di bacino pilota del fiume Serchio. In *Acqua! luoghi, paesaggi, territori, 8, a cura di Ercolini, M.*; ARACNE Editrice: Rome, Italy, 2012; pp. 203–218. [CrossRef]

72. Böhm, W. *Methods of Studying Root System*; Springer: Berlin/Heidelberg, Germany, 1979. [CrossRef]

73. Osticioli, I.; Mencaglia, A.A.; Siano, S. Temperature-controlled portable Raman spectroscopy of photothermally sensitive pigments. *Sens. Actuators B Chem.* **2017**, *238*, 772–778. [CrossRef]

74. Osticioli, I.; Agresti, J.; Fornacelli, C.; Turbanti Memmi, I.; Siano, S. Potential role of LIPS elemental depth profiling in authentication studies of unglazed earthenware artifacts. *J. Anal. At. Spectrosc.* **2012**, *27*, 827–833. [CrossRef]

75. Agresti, J.; Indelicato, C.; Perotti, M.; Moreschi, R.; Osticioli, I.; Cacciari, I.; Mencaglia, A.A.; Siano, S. Quantitative Compositional Analyses of Calcareous Rocks for Lime Industry Using LIBS. *Molecules* **2022**, *27*, 1813. [CrossRef]

76. Osticioli, I.; Ciofini, D.; Banchelli, M.; Capozzoli, L.; Gallo, L.; Lavacchi, A.; Salvadori, B.; Matteini, P.; Siano, S. "Argento Deaurato" or "Argento Biancheggiato"? A Rare and Interesting Case of Silver Background in Italian Painting of the XIII Century. *Appl. Sci.* **2020**, *10*, 2404. [CrossRef]

77. Olori, A.; Di Pietro, P.; Campoiano, A. Preparation of ultrapure Kbr method for FTIR quantitative analysis. *Int. J. Sci. Acad. Res.* **2021**, *2*, 1015–1020.

78. Pandey, K.K.; Pitman, A.J. FTIR studies of the changes in wood chemistry following decay by brown-rot and white-rot fungi. *Int. Biodeterior. Biodegrad.* **2003**, *52*, 151–160. [CrossRef]

79. Ryan, C.G.; Clayton, E.; Griffin, W.L.; Sie, S.H.; Cousens, D.R. SNIP, a statistics-sensitive background treatment for the quantitative analysis of PIXE spectra in geoscience applications. *Nucl. Instrum. Methods Phys. Res. Sect. B* **1988**, *34*, 396–402. [CrossRef]